Automated Determination of Arterial Input Function for DCE-MRI of the Prostate

Yingxuan Zhu[a], Ming-Ching Chang[b], Sandeep N. Gupta[b]
[a]Dept. of EECS, Syracuse University, Syracuse, NY 12304 USA
[b]GE Global Research Center, One Research Circle, Niskayuna, NY 12309 USA
Emails: [a]yingxuan.zhu@gmail.com; [b]{changm, guptas}@research.ge.com

Abstract

Prostate cancer is one of the commonest cancers in the world. Dynamic contrast enhanced MRI (DCE-MRI) provides an opportunity for non-invasive diagnosis, staging, and treatment monitoring. Quantitative analysis of DCE-MRI relies on determination of an accurate arterial input function (AIF). Although several methods for automated AIF detection have been proposed in literature, none are optimized for use in prostate DCE-MRI, which is particularly challenging due to large spatial signal inhomogeneity. In this paper, we propose a fully automated method for determining the AIF from prostate DCE-MRI. Our method is based on modeling pixel uptake curves as gamma variate functions (GVF). First, we analytically compute bounds on GVF parameters for more robust fitting. Next, we approximate a GVF for each pixel based on local time domain information, and eliminate the pixels with false estimated AIFs using the deduced upper and lower bounds. This makes the algorithm robust to signal inhomogeneity. After that, according to spatial information such as similarity and distance between pixels, we formulate the global AIF selection as an energy minimization problem and solve it using a message passing algorithm to further rule out the weak pixels and optimize the detected AIF. Our method is fully automated without training or *a priori* setting of parameters. Experimental results on clinical data have shown that our method obtained promising detection accuracy (all detected pixels inside major arteries), and a very good match with expert traced manual AIF.

1 Introduction

Prostate cancer is one of the commonest cancers in the world with very high incidence and prevalence rates. Dynamic contrast enhanced MRI (DCE-MRI) has shown promise in diagnosis, staging, and monitoring response to therapy, and has the potential to be a non-invasive biomarker of disease [1]. Quantitative analysis of DCE-MRI provides estimates of tumor pathophysiological properties such as permeability, blood volume, and extra cellular volume fraction. This analysis relies on the determination of an arterial input function (AIF), which is an estimate of the contrast agent concentration in the capillaries feeding the tumor. AIF is usually measured in a nearby major artery. Reliably selecting the AIF is one of the most important factors in the accuracy and reproducibility of DCE-MRI.

Manual methods of selecting the AIF are time consuming and suffer from inter-observer variability. Automated AIF detection is desirable for reasons of speed and repeatability. Several methods for automated AIF detection have been proposed in the literature [2, 3, 4, 5]. Most of these methods focus on brain anatomy, and none are optimized for use in prostate DCE-MRI. Prostate DCE-MRI suffers from extreme spatial inhomogeneity in signal intensities due to the use of endo-rectal coils. Therefore, a global signal intensity based method may not be able to detect arterial pixels located far away from the coil. Intensity normalization methods result in amplification of noise and can yield poor results. In this paper, we propose a fully automated method to determine the AIF from prostate DCE-MRI data. Our method is based on the use of gamma variate functions (GVF) which serve as a good approximation of AIF [6], and find the upper and lower bounds for its parameters to restrict the approximated AIF to desired shapes. Next, we set up a model to fit the GVF for each pixel in time dimension from the 4D DCE-MRI data, and eliminate the false positive pixels by using the deduced upper and lower bounds. After that, considering the estimated AIF candidate pixels may represent various large and small vessels, we formulate an energy function to detect AIF by using global information and optimize it using a message passing algorithm [7] to locate the pixels in major arterial vessels.

The advantages of our method can be summarized as follows. First of all, the estimation of parameters in our method is based on analytically computed bounds, which guarantees the generated GVF is consistent with the proper-

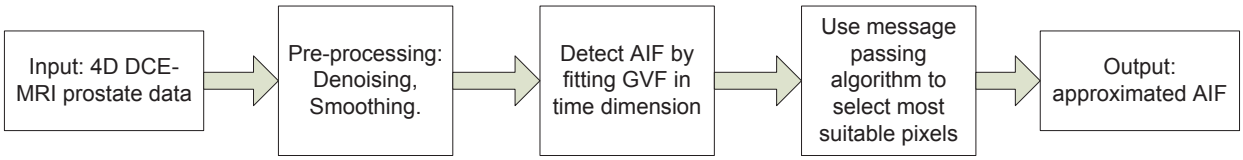

Figure 1: Summary of approach in determination of AIF from DCE-MRI prostate data.

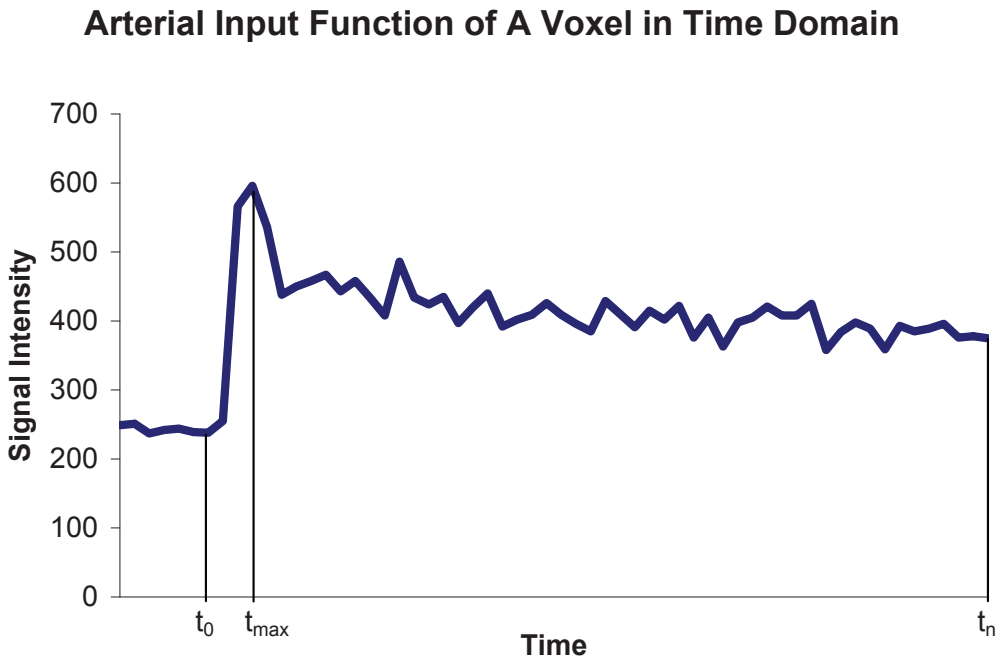

Figure 2: Illustration of a typical AIF curve (signal intensity over time axis).

ties of AIF. Secondly, each pixel of the data is analyzed locally in time dimension, which is robust to global inhomogeneity effect. Third, the message passing algorithm integrates the global information such as similarity and distance between pixels to improve the accuracy of AIF determination. Moreover, our method does not need any training data or *a priori* setting of parameters, and is fully automated.

2 Methods

From DCE-MRI datasets, we extract signal intensity versus time data for 3D volumes depicting wash-in and wash-out of contrast agent concentration. In our method, we use GVF as a reference, and look for pixels which have a good fit with GVF in the time dimension. These pixels will be the candidates to determine the final AIF. Figure 1 shows a summary of our method. After pre-processing which includes denoising and smoothing, the GVF for each pixel is estimated, and unsuitable pixels are ruled out if the parameters of their GVFs are not between the upper and lower bounds. In order to further refine candidate pixels, and only select those that fall in major vessels free of flow and motion artifacts, a message passing algorithm is used to iteratively update the probability of being a suitable AIF candidate for each candidate pixel based on the distance and similarity between pixels. Resulting pixels with larger probabilities are used to determine the final AIF.

Specifically, given a 4D DCE-MRI dataset u, $u(p,t) : \overline{\Omega} \rightarrow \mathbb{R}$ represent the intensity value of point p at time t, where $p = (x, y, z) \in \Omega$ and $\Omega \subset \mathbb{R}^3$. Moreover, t_0 is the bonus arrival time, t_{max} is the time when the AIF obtains its peak value, and t_l is the last observed time. Figure 2 illustrate an AIF curve. Let $g(p,t)$ represent the GVF of pixel p in time domain, $\hat{g}(p,t)$ be the corresponding approximation value of $g(p,t)$ according to $u(p,t)$. In this section, since each pixel has its own GVF fitting curve, we simply use $g(t)$ to represent $g(p,t)$, and $u(t)$ to describe $u(p,t)$.

The GVF for a pixel in time domain can be presented as follows,

$$g(t) = A(t-t_0)^{\alpha} exp(-\frac{(t-t_0)}{\beta}), \tag{1}$$

where $A > 0$, and the paramater α can be determined by the following equation [8],

$$\alpha(t) = \ln(\frac{u(t)}{u(t_{max})})(1 + \ln(\frac{t-t_0}{t_{max}-t_0}) - \frac{t-t_0}{t_{max}-t_0})^{-1}. \tag{2}$$

Here, $u(t)$ is used as $g(t)$ to estimate the parameters for a pixel. The maximum value of the AIF can be obtained by $g'(t) = 0$, i.e., $\alpha\beta = t_{max} - t_0$. Technically, as $u(t)$ is given, a GVF can be estimated for each pixel by Equation (2).

The curve of $g(t)$ in Equation (1) can represent different shapes by varying its parameters. In order to restrict the GVF to typical blood pixel shapes, we deduce the lower and upper bounds of α for $t > 0$ as follows.

Proposition 1.

$$0 < \alpha < t_{max} - t_0. \tag{3}$$

Proof. From Equation (1), we have

$$\frac{g'(t)}{g(t)} = \frac{\alpha}{t-t_0} - \frac{1}{\beta}, \tag{4}$$

where $g'(t) = \frac{g(t+\Delta t)-g(t)}{\Delta t}$, and $\beta = \frac{(t_{max}-t_0)}{\alpha}$. So,

$$\frac{g(t+\Delta t)}{g(t)} = \Delta t(\frac{\alpha}{t-t_0} - \frac{\alpha}{t_{max}-t_0}) + 1. \tag{5}$$

Moreover,

$$\begin{cases} 0 < g(t+\Delta t)/g(t) < 1, & \text{if } t > t_{max} \\ g(t)/g(t-\Delta t) > 1, & \text{if } t < t_{max}, \end{cases} \tag{6}$$

yielding

$$\begin{cases} 0 < \Delta t(\frac{\alpha}{t-t_0} - \frac{\alpha}{t_{max}-t_0}) + 1 < 1, & \text{if } t > t_{max} \\ \Delta t(\frac{\alpha}{t-t_0} - \frac{\alpha}{t_{max}-t_0}) + 1 > 1, & \text{if } t < t_{max}. \end{cases} \tag{7}$$

For $t > t_{max}$ and $0 < \Delta t(\frac{\alpha}{t-t_0} - \frac{\alpha}{t_{max}-t_0}) + 1$, which is

$$\alpha < \frac{(t-t_0)(t_{max}-t_0)}{\Delta t(t-t_{max})}. \tag{8}$$

As $t \longrightarrow +\infty$, and let $\Delta t = 1$ as the step size in time dimension, we have $\alpha < t_{max} - t_0$.

For $t > t_{max}$, and $\Delta t(\frac{\alpha}{t-t_0} - \frac{\alpha}{t_{max}-t_0}) + 1 > 1$, $\Delta t\alpha\frac{t_{max}-t}{(t-t_0)(t_{max}-t_0)} > 0$, so $\alpha > 0$. Similarly, as $t < t_{max}$, we also have $\alpha > 0$.

Overall,

$$0 < \alpha < t_{max} - t_0. \tag{9}$$

□

Next, we show that α can be futher constrained by considering the decrease in GVF signal after t_{max}, i.e., the faster and slower wash-out can be modeled by α. The following proposition can be proven.

Proposition 2.

$$\ln k(1 + \ln(\frac{t_l - t_0}{t_{max}-t_0}) - \frac{t_l - t_0}{t_{max}-t_0})^{-1} < \alpha < (t_{max} - t_0), \text{ if } t > t_{max}. \tag{10}$$

where t_l is the time of the last value, and $k = \frac{u_{t_l}}{u_{t_{max}}}$ is the intensity ratio of the last value and maximum value of a specific pixel in the dataset.

Proof. According to Equation (2),

$$\alpha(1+\ln(\frac{t_l-t_0}{t_{max}-t_0})-\frac{t_l-t_0}{t_{max}-t_0})=\ln(\frac{u(t)}{u(t_{max})}),$$

Since k=$\frac{u(t_l)}{u(t_{max})}<\frac{u(t)}{u(t_{max})}<1$, for $t_l<t<t_{max}$, then

$$\alpha(1+\ln(\frac{t_l-t_0}{t_{max}-t_0})-\frac{t_l-t_0}{t_{max}-t_0})<\ln k.$$

Therefore, as we know $u(t_l)$ and $u(t_{max})$ of the data, with Equation (3), we have another lower bound of α for $t>t_{max}$,

$$\ln k(1+\ln(\frac{t_l-t_0}{t_{max}-t_0})-\frac{t_l-t_0}{t_{max}-t_0})^{-1}<\alpha<t_{max}-t_0. \tag{11}$$

□

Although we are using this method for prostate DCE-MRI, Equation (10) can be used to generalize the method for other application by adjusting parameter k.

We summarize of our algorithm for AIF determination as follows:

- For each pixel, calculate the first and second derivative of the time curve. Determine t_{max} and $y_{t_{max}}$ using the curvature.
- Determine t_0 by searching for the maximum curvature before t_{max}.
- Compute $\alpha(t)$ for $t_0<t<t_{max}+(t_{max}-t_0)$ according to Equation (2), and use their average as α.
- Compare the obtained α with upper and lower bounds as above, and rule out pixels not satisfying the conditions.
- Determine β and A according to $\beta=\frac{(t_{max}-t_0)}{\alpha}$ and $A=u(t_{max})(\frac{e}{(t_{max}-t_0)})^{\alpha}$.
- Use the parameters to generate $\hat{g}(t)$ for all time samples at t.
- Add a constant with heaviside function for the value of $\hat{g}$ after $t=t_{max}+(t_{max}-t_0)$ to optimize $\hat{g}$. This step is done to model the fact that the observed signal curves do not return to zero in the imaging time but show a non-zero baseline.
- Set up an energy function $\mathcal{F}=F_g(\mathbf{v})+\lambda F_d(\mathbf{v})$, where $F_g(\mathbf{v})$ represents the difference between intensity values and the approximated GVFs, $F_d(\mathbf{v})$ represents the distance between pixels, and $\lambda=1$ is an empirically determined constant. Solve this energy function by using a messages passing algorithm to pick the most robust set of pixels located in a major vessel free of motion and flow artifacts. This paper focuses on introducing the GVF fitting algorithm, we refer the reader to [9, 7, 10] for more details about message passing algorithm.

3 Experimental Results

Our method is validated on clinical prostate DCE-MRI datasets from 5 patients. All patients were scanned under IRB approved protocols after informed consent using a clinical 3T GE MRI scanner and an endo-rectal receive coil and standard DCE-MRI protocols.

Figures 3 and 4 show the results of our algorithm on 3 cases. In these figures, each column shows the results of one dataset, and each row displays the results in one aspect. For each case, the figures include one of the original images, 2D views of slices of the AIF pixels determined by our algorithm, the corresponding AIFs and GVFs, the images of Ktrans and IAUC90, which are 2 main accepted parameters from DCE-MRI with best correlation with therapy response clinically. The original images shown in this figures are selected from each 4D dataset, which have clear display of arteries and are very likely to be selected by the user to determine the AIF manually. All these images are shown in original gray scale without any adjustment in intensity values for clear display purpose. The 2D displays show the selected AIF pixels in the original images as green points, where the intensity values of the original images are adjusted for display. The "AUTO AIF" in green of third row of Figure 3 is the AIF determined by calculating the average AIF of the AIF voxels, and the "AUTO GVF" in blue is for the average values of the approximated GVF. The curves of "Manual AIF" in red are obtained by manually selecting the points in artery.

The first row of Figure 3 shows the original images, each one represents a slice in the 4D data at a specific time. From these original images, we can see that the images of 4D prostate DCE-MRI have extreme intensity

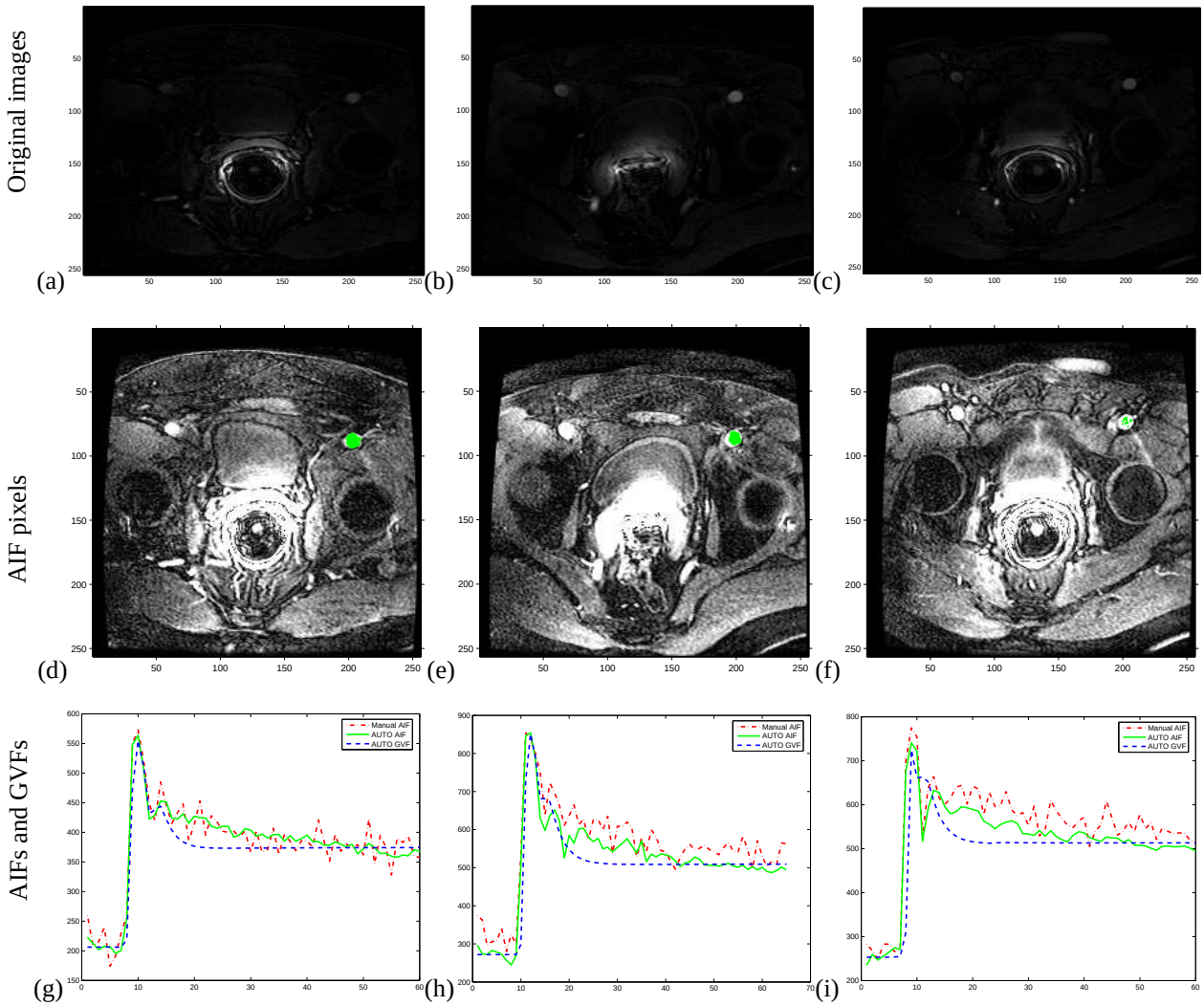

Figure 3: The original images (a)-(c), detected arterial pixels (d)-(f), and the corresponding averages of AIFs and GVFs (g)-(i).

inhomogeneity. Though the original images are all dark, the coil areas of these images are much brighter than any other areas. With contrast agent, the arteries can be recognized in these images, though it may be cumbersome to manually locate an artery in this kind of images in a large 4D dataset. From these images, we can also see the scattering spots of small vessels which are also very bright comparing to the background.

The second row of Figure 3 displays the detected AIF pixels marked in green (all located in the left femoral arteries). These AIF voxels are shown as green points on the corresponding original images. From these images, comparing to the images in the first row, We can see that despite inhomogenous intensity values, the selection of arterial pixels (the green points) are correct and the determined AIFs are very close to the manually selected ones.

The curves of AIF and GVF determined by our method and by manual selection are compared in the right column of Figure 3. In these figures, the approximated GVFs are very close to the AIFs, and the automatic determined AIFs are similar to the manually selected AIFs. According to these results, we can see that the GVF fitting in our algorithm locates the voxels which have curves as AIF's. The message passing algorithm exchanges location and intensity information between AIF candidates, and finally selects the voxels in the arteries to determine the AIF. Moreover, the AIFs determined by manual selection usually only present the AIF voxels in one slice, but the AIFs obtained by our method contain the information of AIF voxels in the whole 4D dataset.

Figure 4 shows the displays of Ktrans and IAUC90 of the automatically and manual determined AIFs, correspond-

ing to each case in Figure 3. From the first to the last row of this figure displays the Ktrans obtained by manual ROI method, Ktrans obtained by our method, IAUC90 determined by manual ROI method and IAUC90 determined by our method, respectively. In this figure, we can see that the IAUC90 images are identical in all cases with manual ROI method and automatic method. And the Ktrans images are largely similar. It is worth mention that, in one of the cases, shown in the first column, the result of automatic AIF Ktran is clearly better than that of manual ROI. This example shows that, the manual ROI may generate large flow artifact in determining AIFs, while our automatic AIF algorithm picks appropriate pixels in vessels to determine the AIF.

We implemented our algorithm in Matlab and performed experiments on a machine with 2.53 GHz CPU with 2G of RAM. The computation took about 30 seconds for each study depending on the size of volume.

4 Summary

In this paper, we have developed a fully automated method for determining the AIF of DCE-MRI prostate data, and validated our method on clinical data. The method uses both temporal and spatial information and is robust to intensity non-uniformity in the prostate DCE-MRI images. The analytically derived GVF parameter bounds significantly increase the accuracy and reduce the computation time. Our method is fully automatic without using any training data or prior information. Moreover, although our method is demonstrated for prostate DCE-MRI, it is directly applicable to other body dynamic data.

References

[1] R. Alonzi, A. R. Padhani, and C. Allen, "Dynamic contrast enhanced MRI in prostate cancer," *European Journal of Radiology* **63**, pp. 335–350, 2007.

[2] M. Rijpkema, J. H. Kaanders, F. B. Joosten, A. J. van der Kogel, and A. Heerschap, "Method for quantitative mapping of dynamic MRI contrast agent uptake in human tumors," *Journal of Magnetic Resonance Imaging* **14**, pp. 457–463, 2001.

[3] K. Murase, K. Kikuchi, H. Miki, T. Shimizu, and J. Ikezoe, "Determination of arterial input function using fuzzy clustering for quantification of cerebral blood flow with dynamic susceptibility contrast-enhanced MR imaging," *Journal of Magnetic Resonance Imaging* **13**, pp. 797–806, 2001.

[4] F. Calamante, M. Mørup, and L. K. Hansen, "Defining a local arterial input function for perfusion MRI using independent component analysis," *Magnetic Resonance in Medicine* **52**, pp. 789–797, 2004.

[5] S. N. Gupta and J. A. Butman, "Automated computation of the vascular input function for dynamic contrast-enhanced MRI of the brain," in *Annual Meeting, International Society of Magnetic Resonance in Medicine*, 2006.

[6] T. Benner, S. Heiland, G. Erb, M. Forsting, and K. Sartor, "Accuracy of gamma-variate fits to concentration-time curves from dynamic susceptibility-contrast enhanced MRI: Influence of time resolution, maximal signal drop and signal-to-noise," *Magnetic Resonance in Medicine* **15**, pp. 307–317, 1997.

[7] J. Sun, N.-N. Zheng, and H.-Y. Shum, "Stereo matching using belief propagation," *IEEE Transactions on Pattern Analysis and Machine Intelligence* **25**, pp. 787–800, 2003.

[8] M. T. Madsen, "A simplified formulation of the gamma variate function," *Phys. Med. Biol.* **37**, pp. 1597–1600, 1992.

[9] J. Pearl, *Probabilistic Reasoning in Intelligent Systems: Networks of Plausible Inference*, Morgan Kaufmann, San Francisco, first ed., 1988.

[10] Y. Zhu, S. Cheng, and A. Goel, "Interactive segmentation of medical images using belief propagation with level sets," in *Proceedings of IEEE International Conference on Image Processing*, 2010.

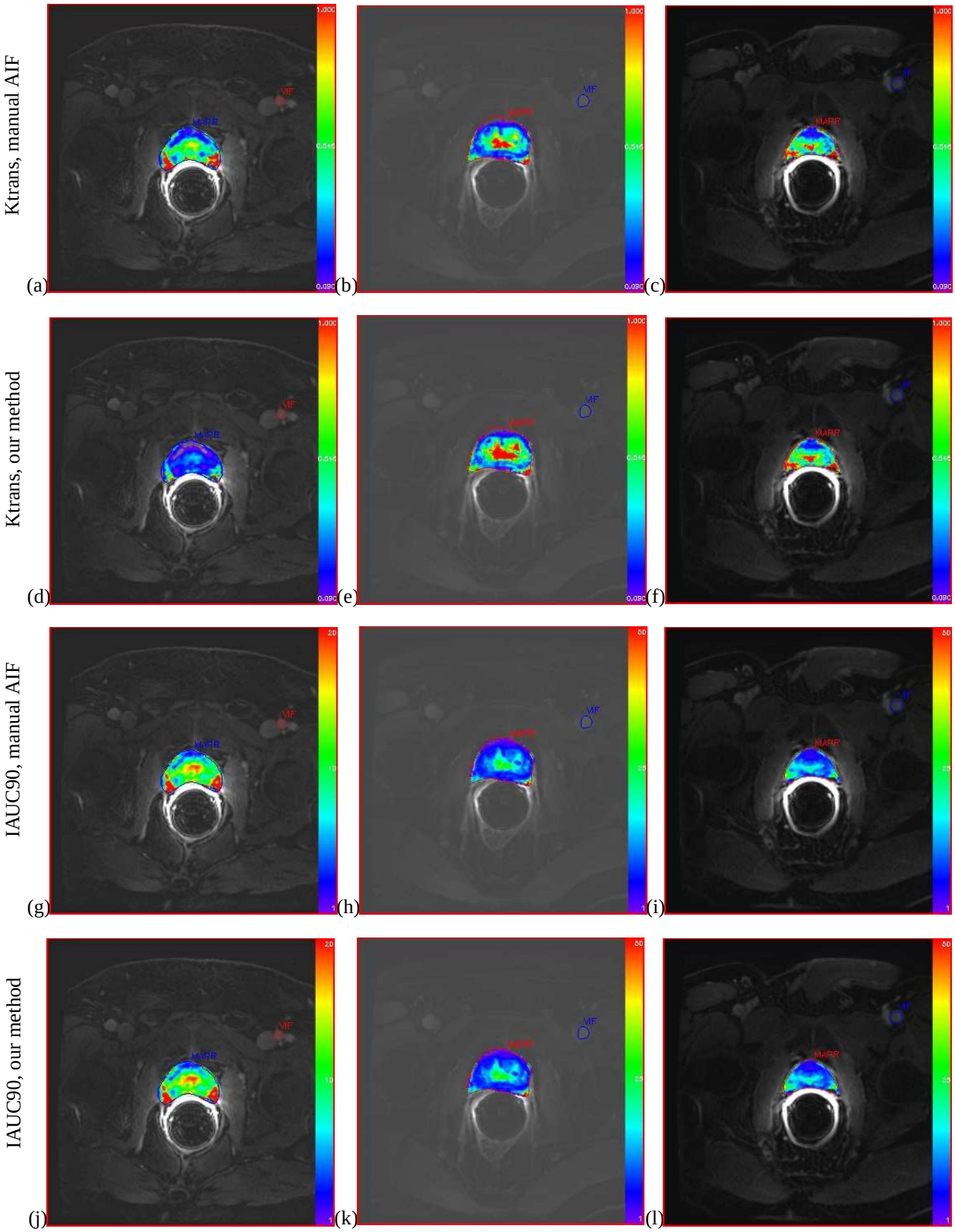

Figure 4: Comparison of Ktrans and IAUC90 determined by our method and manual ROI method.